A Scalable DC Microgrid Architecture for Rural Electrification in Emerging Regions

P. Achintya Madduri, Jason Poon, Javier Rosa, Matthew Podolsky, Eric Brewer, Seth Sanders
Department of EECS
University of California, Berkeley
Berkeley, CA 94720
Email: amadduri@eecs.berkeley.edu

***Abstract*—We present the design and experimental validation of a scalable dc microgrid architecture for rural electrification. The microgrid design has been driven by field data collected from Kenya and India. The salient features of the microgrid are distributed voltage control and distributed storage, which enable developed world grid cost parity. In this paper, we calculate that the levelized cost of electricity (LCOE) for the proposed dc microgrid system will be less than $0.40 per kW-hr. We also present experimental results from a locally installed dc microgrid prototype that demonstrate the steady state behavior, the perturbation response, and the overall efficiency of the system. The experimental results demonstrate the suitability of the presented dc microgrid architecture as a technically advantageous and cost effective method for electrifying emerging regions.**

I. Introduction

There are currently 1.3 billion people in rural developing regions without access to electricity [1]. This number is projected to increase despite increased grid-tied generation since there is still a significant power deficit in urban areas [1]–[3]. Microgrids have been viewed as a viable option to provide electricity for rural areas where the cost of grid extension is prohibitive [4], [5]. In recent years, the falling cost of solar energy has sparked increasing interest in developing renewable methods for rural electrification [6]–[8]. However, battery costs have not declined at the same rate as solar photovoltaic (PV) panels. Since the predominant residential usage is during night-time hours [9], the cost of stored electricity use is a key figure of merit. In this regard, dc microgrids have demonstrated promise as a viable method of enabling improved efficiency and scalability for off-grid systems [8]–[13].

In this paper, we present and experimentally demonstrate a dc microgrid architecture that provides a scalable solution for rural electrification. We calculate the levelized cost of electricity (LCOE) of the described architecture based on BOM costs of the proposed system and field surveys carried out by research partners. We present a hardware prototype setup used to demonstrate the steady state behavior and the perturbation response of the proposed architecture.

This remainder of the paper is organized as follows. Section II presents an overview of the dc microgrid system topology, the distributed control implementation, and LCOE calculations. Section III presents a scaled-down PV-based microgrid prototype used to experimentally demonstrate the operation and stability of the system. Section IV concludes the paper.

II. System Overview and Implementation

In this section, we present an overview of the dc microgrid system architecture and carry out a cost analysis to obtain the LCOE of the proposed microgrid over a 15 year horizon. Additionally, we present a prototype hardware implementation used to experimentally validate the operation and stability of the system.

A. Overview of architecture

An overview of the dc microgrid architecture is shown in Fig. 1. The key components of the system are 1) the maximum power point tracking (MPPT) *source converter*, 2) the *fanout nodes*, and 3) the *household power management units (PMUs)*.

A nominal distribution voltage between 360 and 400 V is used to keep line losses modest while complying with the emerging standards for dc power [14]. The choice also enables use of readily available 600 V power semiconductor devices. The grid voltage is converted to 12 V at the households for storage and appliance use. The *MPPT source converter* is responsible for operating the solar panels at the peak-power point as well as detecting and isolating faults on the grid. The *fanout nodes* aggregate usage from a local cluster of houses (3-5 households within a 15 m radius) and switch and meter the usage of individual households connected to the line. This functionality helps deter theft of power and isolates faults on the grid. Also each fanout node incorporates a fixed ratio 8:1 dc bus converter. The bus converters, which have a rated efficiency of 95%, are commercially manufactured devices typically used in data center applications [15]. They also provide galvanic isolation to the connected households which is an important safety consideration. The fanout node provides an intermediate (45-50 V) bus to the local cluster of houses. Since the fanout nodes use a fixed ratio converter, the information implicit in the grid voltage level is preserved and passed on to the households downstream. Finally, each household interfaces to the microgrid through a *household power management unit (PMU)*, which converts the 45-50 V fanout bus voltage to 12 V through a buck converter for all household appliances, and also integrates battery storage. In addition, the PMUs can digitally communicate information

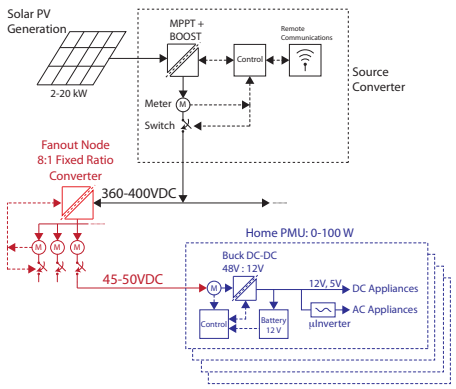

Fig. 1. An architectural overview of the dc microgrid system.

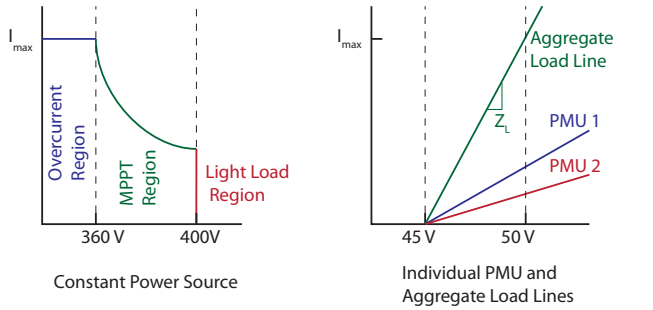

Fig. 2. Source and load impedances. The PMU load-line slope and offset are controllable variables.

such as price, charge-state of households, credits, and usage both locally to the end-user and remotely to the system operator.

A salient property of the dc microgrid architecture is the distributed control of the grid voltage, which enables both instantaneous power sharing and a metric for determining the available grid power. A droop voltage power-sharing scheme is implemented, as shown in Fig. 2, wherein the bus voltage droops in response to low-supply/high-demand. This droop profile is a result of a constant power source which is formed when an MPPT converter is connected to a solar PV panel. The PMUs have a controllable usage profile (load-line) that can can reduce power drawn from the grid by using locally stored energy for the battery to power connected household loads. Switching converters regulated to implement a load-line profile have been shown to have the properties of both large-scale and incremental passivity [8]. Interconnected networks of passive converters have been shown to be stable using energy-based (Lyapunov) techniques [16].

Additionally, the architecture of the dc microgrid aims to minimize the losses associated with stored energy. Since storage is distributed to the individual household PMUs, the number of conversion steps and line losses are reduced. Distributed storage provides reliable provision of electricity 24/7 and also allows for household loads to be decoupled from the grid supply when required. Furthermore, household ownership of batteries enables flexible, demand-driven growth of storage in the grid, since each household makes decisions about the size of the stored supply based on desired night-time usage.

B. Levelized Cost of Electricity Calculations

The levelized cost of electricity (LCOE) is calculated based on the specifications shown in Table II. Cost assumptions of Fanout Nodes and PMUs were based on BOM costs of components used in the prototype system at low production volumes (500 units). A 15 year time horizon was used based on rated lifetimes of solar panels and the power converter components. Lithium Iron Phosphate (LFP) batteries were used to calculated storage costs due to having a favorable combination of longer cycle life and higher safety in comparison to other lithium-ion chemistries [17]. Over a 15 year window it is assumed that the LFP batteries would have to be replaced twice with an estimated cycle life of greater than 2000 cycles without significant loss of capacity [18]. Wiring costs were estimated based on using aluminum distribution wire sized at keeping voltage drop across 1 km under 3% at full load. The calculated LCOE of the dc microgrid is favorable in comparison to presently deployed solar microgrid systems and also with grid power rates on certain Hawaiian islands [19].

C. Prototype implementation

In order to experimentally validate the proposed dc microgrid architecture, a scaled-down 400 W hardware prototype setup, shown in Fig. 3a, was constructed and installed at the University of California, Berkeley. The full specifications and ratings for the prototype setup are presented in Table I.

The converter designs and enclosures are shown in Fig. 3. The MPPT source converter (Fig. 3b) consists of a 2-phase interleaved boost converter, fuse protection, and connectors for PV input and bus output. The fanout node is implemented using a commercially available 8:1 fixed ratio 300 W dc converter which converts from 360-400 V to 45-50 V. The household PMU (Fig. 3c) consists of a 100 W synchronous buck converter, fuse protection, 100 W-hrs of battery storage, and connectors for 45-50 V bus input and 12 V dc output. The load-line is implemented using proportional feedback of voltage at the input terminal of the converter as shown in Fig. 4. The output from the outer voltage loop forms the reference to the inner current loop. The gain of the outer loop determines slope of the load-line (input impedance) of the converter. Achieving load-line regulation through such a proportional feedback scheme has been used for output regulation of dc-dc converters [20], [21]. We use the same techniques to achieve load-line regulation on the input of the PMU buck converters.

III. Experimental Results

In this section, we present experimental results that demonstrate the operation of the dc microgrid prototype setup under various operating conditions. The steady state behavior of the PMU converters, and the perturbation response of grid voltage are shown as the power from the source is varied. The startup

TABLE I
SPECIFICATIONS AND RATINGS FOR PROTOTYPE MICROGRID

Solar PV array	
Rated power	400 W
Rated open circuit voltage	200 V
MPPT Source Converter	
Topology	2-phase boost converter
Rated power	400 W
Rated output voltage	400 V
Switching frequency	100 kHz
Household PMU	
Topology	Synchronous Buck
Rated power	100 W
Rated output voltage	12 V
Switching frequency	250 kHz

TABLE II
LCOE PARAMETERS AND CALCULATION OVER A 15 YEAR HORIZON

System Parameters	
Number of Households	100
Daily Usage	100 W-hrs/day
Radius of Microgrid	1 km
Generation Costs	
Rated Size of Solar Panels	2 kW
Cost of Solar Panels	\$0.70 per W
Cost of Source Converter	\$0.25 per W
Total Cost of Generation	\$1,900
Fanout Node Costs	
No. of Fanout nodes in system	30
Cost of Fanout nodes	\$0.20 per W
Total cost of Fanout nodes	\$2,000
PMU Costs	
Power rating of individual PMU	100 W
Cost of PMUs	\$0.15 per W
Total Cost of PMUs	\$1,500
Battery Costs	
Storage per household	100 W-hrs
LFP Battery Cost	\$0.50 per W-hr
Total Battery Costs over 15 years	\$10,000
Wiring Costs	
Total T&D wiring costs	\$4,000
Total System Cost	\$19,400
LCOE of elec. delivered over 15 years	\$0.35 per kW-hr

and shutdown behaviors of the various components of the grid are also shown.

A. Experimental Test Setup

A solar panel connected to a MPPT converter behaves as a constant power source. In order to create a controllable constant-power-source for the experiments in this section, a boost converter operating in input-current-control mode was used, i.e., where the input current from the voltage source is controlled. A schematic of the setup is shown in Fig. 5. The input power to the grid can be varied by either by changing the input voltage to the current-controlled boost or by changing the current command. A change in the current command was used to cause step changes in grid power.

B. Steady State Behavior

Fig. 6 shows the steady-state response of the PMU input current as a function of the grid voltage. The efficiencies of the Fanout and PMU converters used in the experiment setup

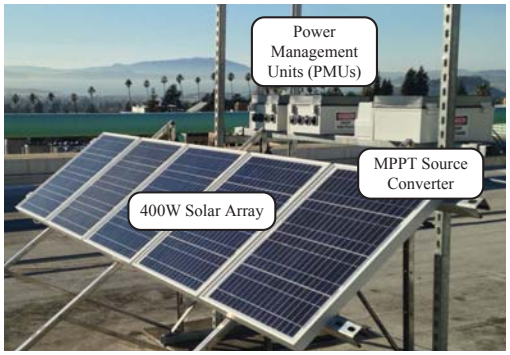

(a) The scaled-down dc microgrid prototype used for experimental validation.

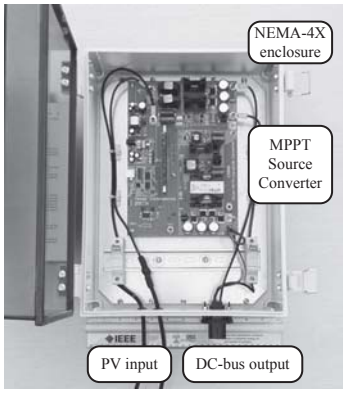

(b) MPPT source converter.

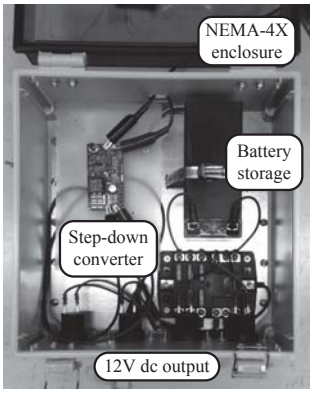

(c) Power management unit (PMU).

Fig. 3. Photographs of dc microgrid prototype setup and components.

are shown in Fig. 7. Both simulation and experimental results show the same relationship between current drawn by the PMU and input voltage. As shown, the current drawn by each PMU increases as the grid voltage increases, thus exhibiting a positive impedance characteristic. The slope of this load-line is fully programmable and set by the feedback gain of input voltage. The gain on the controller is set to achieve an input impedance of $Z = 2\ \Omega$. Once the PMU converter is operating in continuous conduction mode, both the simulation and experiment show that the steady state input impedance is $2\ \Omega$. When the converter is in discontinuous conduction mode, the input impedance is higher than idealized case. However,

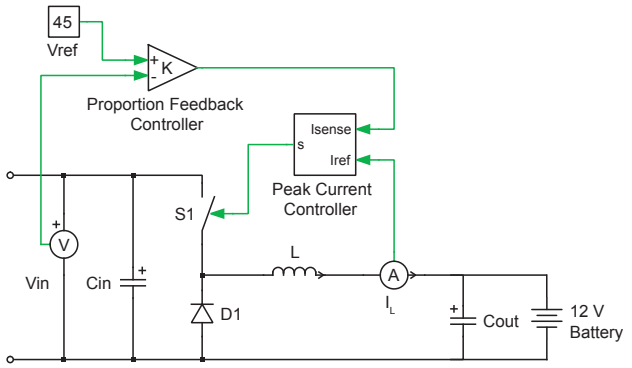

Fig. 4. PMU Load-line Implementation. The gain of the outer voltage loop sets the load-line slope.

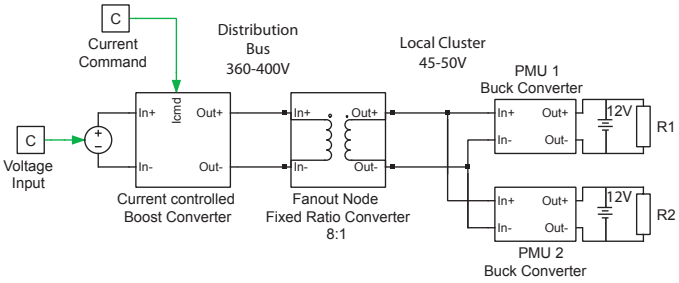

Fig. 5. Schematic of Experimental Setup.

this deviation does not have any significant impact on system behavior as will be shown by the perturbation response.

C. Perturbation Response

Fig. 8 shows the perturbation response of the grid voltage, fanout node voltage, and the input current to the 2 PMUs in response to a step change in the available grid power. Initially, the input power to the grid is 5 W. At this level, the fanout node is powered on, but the fanout bus voltage is below 45 V so the PMUs are not drawing any current from the grid; the power is dissipated in the fanout node bus converter. At $t = 0.19$ s, the available grid power is instantaneously increased from 5 W to 70 W by commanding a step change in input current drawn by the boost converter in the experimental setup (Fig. 5). Immediately, the grid voltage starts to rise, but remains within the 360 to 400 V range. This stabilization is due to the response of the PMUs, which increase their current draw in response to the increase in grid voltage.

D. Startup and Shutdown Behavior

Fig. 9a shows the startup behavior of the microgrid. After the power source is turned on, the voltage on high voltage bus of the grid starts to rise. The high voltage bus rises to 400 V before the fanout node starts to operate. Upon turn on of the fanout node BCM, $t = 1$ sec, the voltage on the fanout node bus immediately rises to 50 V. The initial spike in PMU current is due to the input capacitors charging from 0 to 50 V. The PMUs connected to the fanout node start to draw current from the fanout bus according to their load-line.

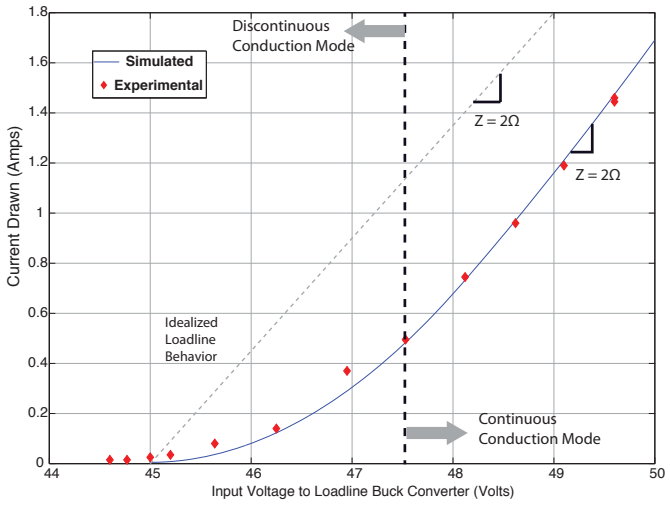

Fig. 6. Simulation and experimental results showing the change in input current of a PMU buck converter implementing a load-line profile in response to grid voltage on the fanout node bus.

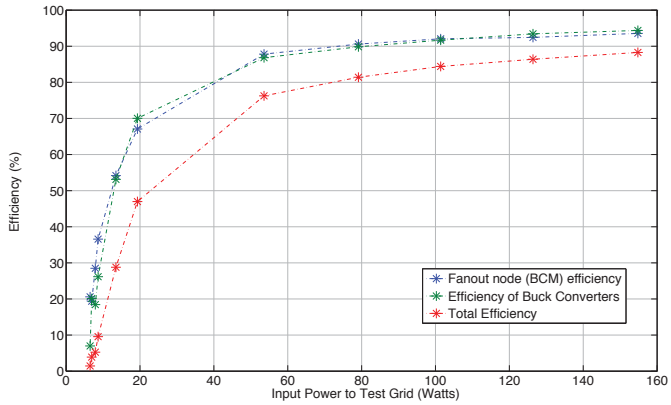

Fig. 7. Efficiency of the Fanout Bus Converter and PMU Buck converters as a function of input power for the configuration shown in Fig. 5.

This subsequently causes the voltage on both busses to droop and settle at an operating point determined by the available power and the slope of the aggregate PMU load-line.

Fig. 9b shows the shutdown behavior of the microgrid. As the bus voltages start to drop, the PMUs respond by drawing less current from the grid. Once the fanout bus voltage drops below 45 V, the PMUs do not draw any more current. As the grid voltage drops below 300 V the bus converter in the fanout nodes also shuts down and the grid voltage continues to fall. In both startup and shutdown scenarios, the household load on the low-voltage side of the PMU is decoupled due to the battery.

IV. Conclusions

This paper presented the design and implementation of a scalable dc microgrid architecture for rural electrification. The cost analysis of the system shows that over a 15 year time span, the LCOE can be below $0.40 per kWh. This provides a compelling case for the economic viability of the architecture, an important consideration in rural emerging regions.

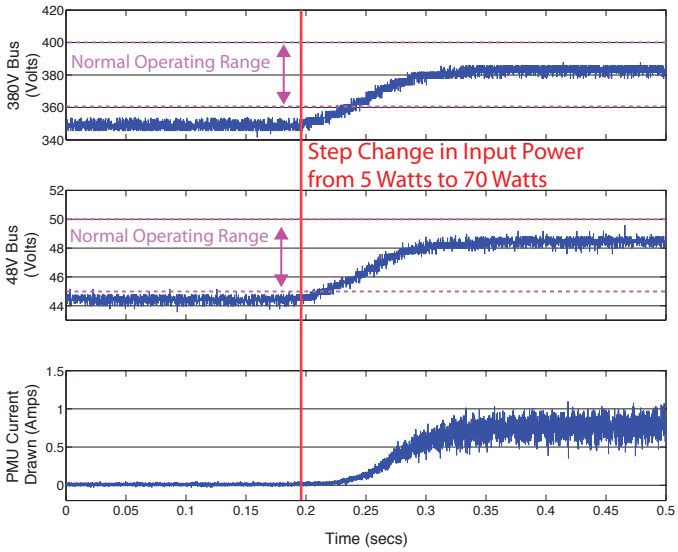

Fig. 8. Transient behavior of bus voltages and PMU current draw in response to a step increase in grid power (5 W to 70 W) at time $t = .19$ secs.

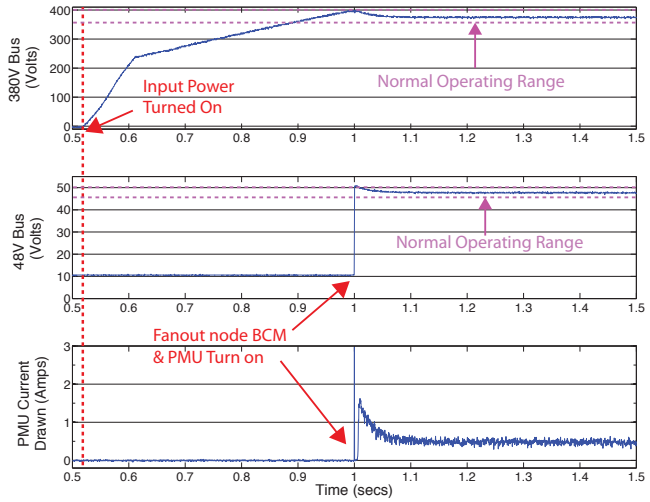

(a) Startup behavior of experimental microgrid setup after input voltage source is turned on at time $t = .52$ secs. The available power from the source upon startup is 55 W

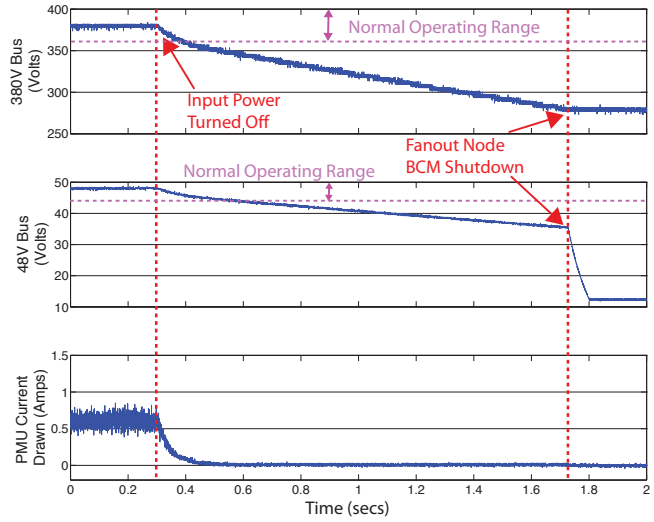

(b) Shutdown behavior of experimental microgrid setup after input voltage source is turned off at time $t = .3$ secs.

Fig. 9. Startup and shutdown behavior of prototype dc microgrid system with input power set to 55 W.

We experimentally demonstrated the operation and stability of the dc microgrid with distributed voltage control. The load-line control scheme implemented by the PMUs enables integration of completely variable sources and requires minimal regulation overhead. Relative ratios of load-lines determine the power-sharing between the different PMUs, thereby allowing for load prioritization.

The dc microgrid described in this paper allows for maximizing efficiency of stored electricity, a key figure of merit for off-grid system. The architecture shows promise in addressing the economic and technical challenges of electrifying rural emerging regions.

Acknowledgment

This work was supported by the Blum Center for Developing Economies, Berkeley Energy and Climate Institute, and the Development Impact Lab (USAID Cooperative Agreement AID-OAA-A-12-00011), part of the USAID Higher Education Solutions Network.

References

[1] "Energy for all: financing access for the poor," tech. rep., IEA World Energy Outlook, 2011.

[2] L. Srivastava and I. H. Rehman, "Energy for sustainable development in India: Linkages and strategic direction," *Energy Policy*, vol. 34, pp. 643–654, Mar. 2006.

[3] M. Nouni, S. Mullick, and T. Kandpal, "Providing electricity access to remote areas in India: An approach towards identifying potential areas for decentralized electricity supply," *Renewable & Sustainable Energy Reviews*, vol. 12, pp. 1187–1220, June 2008.

[4] Z. Ding, M. Liu, W.-J. Lee, and D. Wetz, "An autonomous operation microgrid for rural electrification," in *2013 IEEE Industry Applications Society Annual Meeting*, pp. 1–8, IEEE, Oct. 2013.

[5] T. Levin and V. M. Thomas, "Least-cost network evaluation of centralized and decentralized contributions to global electrification," *Energy Policy*, vol. 41, pp. 286–302, Feb. 2012.

[6] S. C. Bhattacharyya, "Review of alternative methodologies for analysing off-grid electricity supply," *Renewable and Sustainable Energy Reviews*, vol. 16, pp. 677–694, Jan. 2012.

[7] D. Soto, E. Adkins, M. Basinger, R. Menon, S. Rodriguez-Sanchez, N. Owczarek, I. Willig, and V. Modi, "A prepaid architecture for solar electricity delivery in rural areas," in *Proceedings of the Fifth International Conference on Information and Communication Technologies and Development - ICTD '12*, (New York, New York, USA), p. 130, ACM Press, Mar. 2012.

[8] P. A. Madduri, J. Rosa, S. Sanders, E. Brewer, and M. Podolsky, "Design and verification of smart and scalable DC microgrids for emerging regions," *2013 IEEE Energy Conversion Congress and Exposition*, pp. 73–79, Sept. 2013.

[9] D. Soto and V. Modi, "Simulations of Efficiency Improvements Using Measured Microgrid Data," *Global Humanitarian Technology Conference (IGHTC), 2012 IEEE*, pp. 369–374, 2012.

[10] D. Boroyevich, I. Cvetkovic, D. Dong, R. Burgos, F. Wang, and F. Lee, "Future electronic power distribution systems a contemplative view," in *2010 12th International Conference on Optimization of Electrical and Electronic Equipment*, pp. 1369–1380, IEEE, May 2010.

[11] W. Jiang and Y. Zhang, "Load Sharing Techniques in Hybrid Power Systems for DC Micro-Grids," *Power and Energy Engineering Conference*

(APPEEC), 2011 Asia-Pacific, pp. 1–4, 2011.

[12] W. Zhang, D. Dong, I. Cvetkovic, F. Lee, and D. Boroyevich, "Lithium-based energy storage management for DC distributed renewable energy system," *Energy Conversion Congress and Exposition (ECCE), 2011 IEEE*, pp. 3270–3277, 2011.

[13] L. Zhang, T. Wu, Y. Xing, K. Sun, and J. M. Gurrero, "Power control of DC microgrid using DC bus signaling," in *2011 Twenty-Sixth Annual IEEE Applied Power Electronics Conference and Exposition (APEC)*, pp. 1926–1932, IEEE, Mar. 2011.

[14] "Emerge Alliance.," [Online] Available: http://www.emergealliance.org.

[15] "Vicor BCM Bus Converter Module," [Online] Available: http://www.vicorpower.com/dc-dc-converters-board-mount/bus-converter-module.

[16] S. Sanders and G. C. Verghese, "Lyapunov-based control for switched power converters," *Power Electronics, IEEE Transactions on*, vol. 7, no. 1, pp. 17–24, 1992.

[17] "A-123 Lithium Iron Phosphate Batteries.," [Online] Available: http://www.a123systems.com/lithium-iron-phosphate-battery.htm.

[18] E. M. Krieger, J. Cannarella, and C. B. Arnold, "A comparison of lead-acid and lithium-based battery behavior and capacity fade in off-grid renewable charging applications," *Energy*, vol. 60, pp. 492–500, Oct. 2013.

[19] "Electric Rates for Hawaii Electric Light.," [Online] Available: http://www.hawaiielectriclight.com/helco/Residential-Services/Electric-Rates.

[20] A. V. Peterchev and S. R. Sanders, "Load-Line Regulation With Estimated Load-Current Feedforward: Application to Microprocessor Voltage Regulators," *Power Electronics, IEEE Transactions on*, vol. 21, no. 6, pp. 1704–1717.

[21] R. Redl and N. O. Sokal, "Near-Optimum Dynamic Regulation of DC-DC Converters Using Feed-Forward of Output Current and Input Voltage with Current-Mode Control," *Power Electronics, IEEE Transactions on*, no. 3, pp. 181–192, 1986.